

QUARTZ-SAND COMPRESSIBILITY AT HIGH STRESSES AND TEMPERATURES

STISLJIVOST KREMENOVEGA PESKA PRI VISOKIH OBREME-NITVAH IN TEMPERATURI

Miriam Martín-Ruiz

Universidad Politécnica de Madrid, UPM,
Department of Continuum Mechanics and Structures
Madrid, Spain
E-mail: miriam.martin@alumnos.upm.es

José Alvarellós

Repsol
Madrid, Spain
E-mail: jose.alvarellós@repsol.com

Jordi Delgado

University of A Coruña,
Department of Civil Engineering
A Coruña, Spain
E-mail: jorge.delgado@udc.es

José María Goicolea

Universidad Politécnica de Madrid,
Department of Continuum Mechanics and Structures
Madrid, Spain
E-mail: jose.goicolea@upm.es

DOI <https://doi.org/10.18690/actageotechslov.16.2.39-49.2019>

Keywords

compressibility, particle crushing, temperature effect, high-stresses effect, subcritical cracking growth

Ključne besede

stisljivost, drobljenje delcev, temperaturni učinek, učinek visokih obremenitev, rast mejne kritične razpoke

Abstract

The effects of temperature on the degree of grain crushing and the stress-strain response of a granular soil subjected to high stresses are a matter of interest for unconventional geomechanical projects. As a part of a research program on the thermo-hydro-mechanical-chemical compressibility of quartz sand from a heavy oil reservoir, we have conducted a series of oedometric tests under dry conditions, high stresses (up to 50 MPa) and constant temperatures, ranging from 25 to 250°C. Acoustic emissions were recorded throughout the tests, and SEM photomicrographs of sieved grain-size fractions before and after the experiments were analysed.

The results show that the temperature has a negligible effect on the macroscopic compressibility, with similar oedometric curves for all the tests. Conversely, the acoustic-emission counts drop off, and changes in the particle size distribution are minor, though grains subjected at high temperature show incipient fractures attributed to subcritical cracking through stress-corrosion.

Izvleček

Za nekonvencionalne geomehanske projekte je zanimiv vpliv temperature na stopnjo drobljenja zrn in napeto-stno-deformacijski odziv zrnatih zemljin, izpostavljenih visokim obremenitvam. Kot del raziskovalnega programa o termo-hidromehansko-kemijski stisljivosti kremeno-vega peska iz težkega naftnega rezervoarja so avtorji izvedli serijo edometriških preizkusov pri suhih pogojih, visokih obremenitvah (do 50 MPa) in konstantnih temperaturah v razponu od 25 do 250 °C. Med preizkusi so bile zabeležene akustične emisije in analizirane SEM fotomikrografije presejanih frakcij velikosti zrn pred in po preizkusih

Rezultati kažejo, da ima temperatura zanemarljiv vpliv na makroskopsko stisljivost, pri podobnih krivuljah stisljivosti za vse preizkuse. Nasprotno pa število akustičnih emisij upada in so spremembe v porazdelitvi velikosti delcev manjše, čeprav zrna, izpostavljena visoki temperaturi, kažejo začetne lome, ki se pripisujejo mejnemu kritičnemu razpokanju zaradi napetostne korozije.

Thus, the compressibility of the samples tested at high and low temperatures can be explained within the same grain-scale mechanisms of cracking: critical rapid Herzian crack growth, at low temperatures, and subcritical silent crack growth by stress-corrosion, at the higher temperatures.

Tako lahko stisljivost vzorcev, preizkušenih pri visokih in nizkih temperaturah, razložimo z enakimi mehanizmi razpoka v velikosti zrna: kritična hitra Hertzianova razpoka raste pri nizkih temperaturah, medtem, ko mejna kritična tiha razpoka zaradi napetostne korozije raste pri višjih temperaturah.

1 INTRODUCTION

While geotechnical practice does not typically require a knowledge of temperature effects, emerging geoenvironmental and geomechanical applications require a knowledge of the grain crushing in soils and granular materials under high stresses and temperatures. Examples of this kind are thermal oil recovery in petroleum engineering, CO₂ capture and storage (CCS), storage of radioactive waste and unconventional foundations or structures.

The compressibility and crushing of quartz sand at high pressures, considered either as an assembly of single particles or as a bulk skeleton, have been examined using compression (or oedometric) data for quartz sands, plotted as $e - \log \sigma_v$ curves and the identification of a stress threshold that leads to a steepening of its slope at high stresses.

While large stresses have been achieved, the effects of temperature on compressibility and grain cracking require further study. The point of maximum curvature, commonly known as the yield point, is a stress level that marks the onset of particle crushing. Particle rearrangement and packing are the main sources of strains at low loads (conventional geotechnics); as the stress increases, the early asperity damage leads to particle splitting. Beyond that stress threshold, the compression curve fits into a linear relationship in the semi-log plot, called the normal (or virgin) compression line [1-5], which can be thought of as a "degenerated-by-crushing" normal compression line (provided the tests can be carried out at room temperature), in contrast to the classic concepts.

The initial void ratio, grain shape, size, and grading govern the compressibility of quartz sands and, particularly, the yield point [5-11]. The high rates of loading intensify the grain crushing as well [12-17].

Related processes have been dealt with, on the one hand, in the scope of Earth Sciences, such as the diagenetic compaction of natural sediments [18-24] and the behaviour of cataclastic zones [25].

2 PURPOSE AND EXPERIMENTAL PROGRAM

Here, we examine the coupled thermo-hydro-mechano-chemical response of quartz sand, saturated with brine and oil, and apply the results to reservoirs in the Orinoco Heavy Oil Belt of Venezuela. A series of 20 compression tests at high stresses (up to 50 MPa) were performed over a range of constant temperature (from 25 to 250°C) in a special oedometric apparatus. Dry conditions were required to assess the effect of the temperature on the sand compressibility at high stresses. In addition, acoustic emissions (AEs) were recorded throughout the oedometric tests, since crushing is the basic acoustic source expected. The samples were examined using a scanning electron microscope (SEM) and an optical microscope.

3 MECHANICAL RESPONSE OF SAND AGGREGATES

When a sand aggregate is subjected to high stresses at room temperature in an oedometric cell, three compressional curvatures or stages can be distinguished along the oedometric curve, as shown in Fig. 1, from [26, 27 and 28].

Particle rearrangement, Stage I

The curvature of the oedometric curve in this stage accounts for the primary compressibility, caused by particle rearrangement, up to the maximum particle packing. Despite the highly constrained conditions of the oedometric cell (radial strains remain zero), the maximum density (maximum packing) is reached as long as the vertical stress is raised up to an intermediate level (5–10 MPa). Hence, the curvature and the slope during this stage depend on the original grain size distribution, the grain morphology and the initial void ratio.

Yield point, Stage II

Once the maximum particle packing is reached, the potential grain movement is completely frustrated and blocked; this state is commonly known as the yield point. The applied stresses are transmitted as discrete

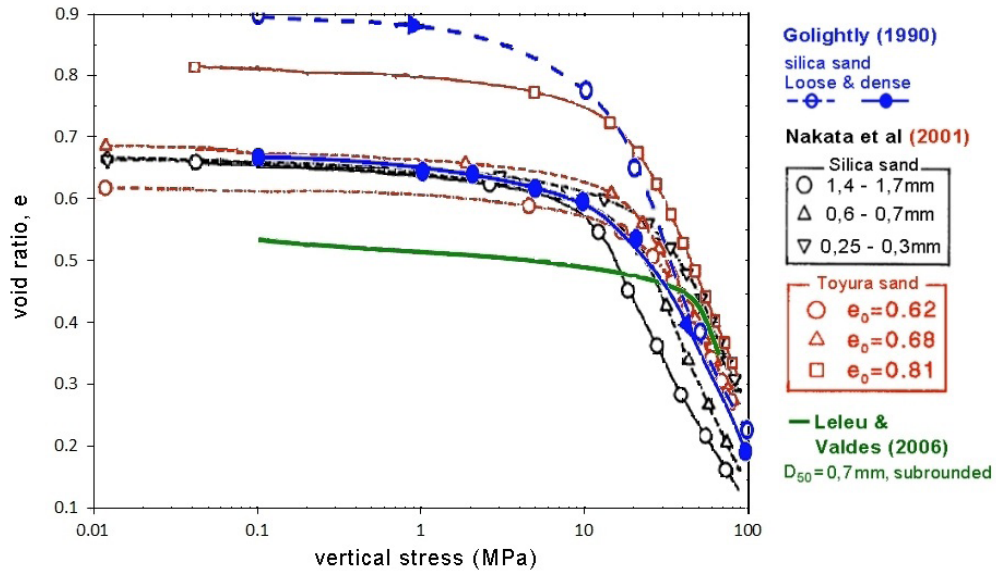


Figure 1. Oedometric curves of quartz sand at high stresses and room temperature (from [26, 27 and 28]).

forces along the grain contacts within the soil skeleton [29]. Therefore, further strains can only occur as a result of particle crushing, which can be addressed appropriately with the concurrence of the following theories.

Hertzian contact theory and critical pressure

Macroscopic yielding depends on the crack initiation at loaded grains and can be examined on the scale of individual contacts between pairs of grains according to the Hertzian theory for loaded spherical bodies. The contact area of the loaded spherical bodies is circular and its radius ($\frac{d_c}{2}$) depends on the normal force applied (F_n), the grain radii (R) and the Young's moduli (E), given by Equation 1 for two identical grains (adapted from [30]).

$$\frac{d_c}{2} = \left(\frac{3 F_n R}{4 E} \right)^{1/3} \quad (1)$$

Even though relevant research efforts in the field of granular media have been made during the past decade to establish the relationship between the macroscale ("Terzaghi" effective) stresses and the microscale (particulate level) stresses, the simplified equation for monosized spheres (Eq. 2) suffices for the purpose of the current research [31 and 32]. The total normal force applied at the contact (F_n) can be expressed as a function of the grain size (d), the normal applied stress (σ) and the void ratio (e).

$$F_n = \sigma(d)^2 \frac{\pi(1+e)^2}{12} \quad (2)$$

The mean intergranular stress at the grain contacts (σ_{int}) can be expressed according to Equation 3.

$$\sigma_{int} = \left(\frac{F_n}{\pi \left(\frac{d_c}{2} \right)^2} \right) \quad (3)$$

Taking into account that the intergranular stress is several orders of magnitude higher than its corresponding effective stress, grains are likely to crush beyond the yield point (with intergranular stresses in the range of 1GPa), leading to a reduction of the mean grain size and the production of fines.

The Hertzian maximum tensile radial stress at the contact (σ_t) reaches its maximum value at the edge of the circular contact area.

$$\sigma_t = \frac{(1-2\nu)\sigma_{int}}{2} \quad (4)$$

The Mode-I stress-intensity factor governs the development of this kind of cracking at the tip of the crack [33], K_I , and follows equation 5 [33 and 34], where c is the length of a pre-existing flaw.

$$K_I = 1.12 \sigma_t \sqrt{\pi c} \quad (5)$$

The crack growth that can ultimately cause the grain failure will only occur if the stress-intensity factor on the tip of the crack reaches the value of the fracture toughness.

$$K_I = K_{IC} \quad (6)$$

Thus, if the Hertzian and the fracture-mechanics models are combined, the pressure of breakage (P_{cr}) [13] can be obtained, which depends on the grain radius, the elastic parameters (E and ν), the porosity (n), or the void ratio, and the properties of the fracture mechanics (K_{IC} , the

fracture toughness and c , the length of the initial pre-existing flaw).

$$\frac{P_{cr}}{E} = 2.2 \frac{(1-\nu^2)^2}{(1-2\nu)^3} \left(\frac{K_{IC}}{E}\right)^3 (\alpha n R)^{-\frac{3}{2}} \quad (7)$$

$$\alpha = \frac{c}{R} \quad (8)$$

Since α is approximately 3.6×10^{-5} for most porous soils [13] and the range of variation of porosity (or void ratio) is relatively narrow, the onset of grain crushing, i.e., when σ_t reaches P_{cr} , is just a function of the grain radius. Thus, the coarser the grains are, the lower the critical pressure of breakage.

Note that, leaving the formulation itself aside, the smaller the particles, the lower the likelihood of the presence of a pre-existing flaw and, therefore, any further development of the crushing.

The microscopic and the macroscopic realms can be connected, and the tensile stress on a particle embedded in a soil matrix due to the normal stress depends on the void ratio [32].

$$\sigma_t = \sigma \left(\frac{(1+e)\pi}{6} \right)^{\frac{2}{3}} \quad (9)$$

Moreover, Field [34], who studied granular assemblies of rounded stones with different sizes and gradings, concluded that the coordination number (the average number of contact points per particle, C_n) varies inversely with the void ratio, as shown in Equation 10.

$$C_n = \frac{12}{1+e} \quad (10)$$

Hence, the tensile stress on a particle in a soil matrix decreases, as shown Equation 11, as the coordination number increases.

$$\sigma_t = \sigma \left(\frac{2\pi}{C_n} \right)^{\frac{2}{3}} \quad (11)$$

Particle breakage and interparticle slip (no thermally induced effect), Stage III

From the moment the overloaded particles start to break, a crushing knock-on effect is triggered, and the compressibility curve shifts to a steeper “degenerated-by-crushing” virgin compression line due to particle crushing and interparticle slip.

Uniform soils made up of coarse particles are more prone to crushing than soils made of finer particles of the same

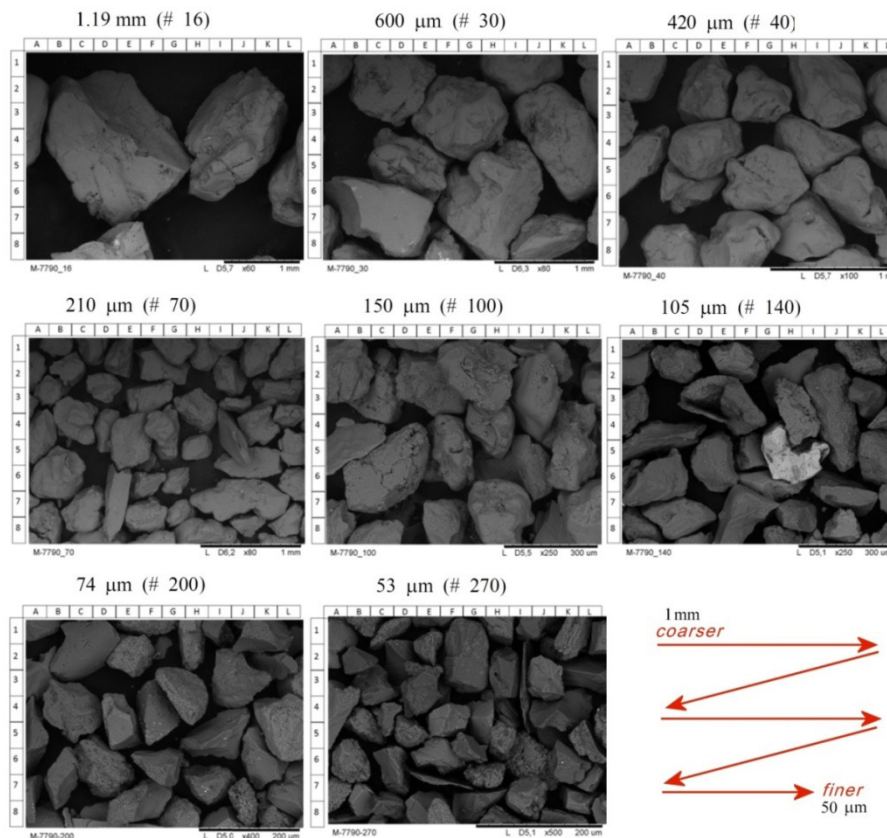


Figure 2. SEM photomicrographs of 8 sieved fractions after cleaning.

material [3, 6, 7, 9 and 10]. Likewise, angular particles are more crushable than rounded particles [3, 7 and 9] as their intergranular stresses tend to be more localised and the asperities favour the locking effect, preventing further packing. Besides, uniform soils exhibit more crushing than well-graded soils having the same maximum size [3 and 9].

Much of our understanding of the compressibility of sand aggregates is restricted to room-temperature loading. This paper takes the theoretical framework of room-temperature compaction, and we examined the compaction at higher temperatures.

4 MATERIAL AND METHODS

4.1 Quartz-sand preparation and characterisation

The sand samples were retrieved from an oil well at a depth of approximately 1000 m. They are fine-grained ($D_{50} \approx 210 \mu\text{m}$), uniform ($c_u \approx 1.8$), uncemented sands, composed of quartz. Prior to testing, oil and any other impurities were removed according to the following

cleaning guidelines: thorough acid-washing (36 wt. % HCl); rinsing with deionised water, and re-washing (96 wt. % ethylic alcohol). Finally, the sand samples were oven-dried. The SEM photomicrographs of 8 different sieved fractions after cleaning are shown in Fig. 2. The photomicrographs suggest that the coarser fractions contain sub-rounded grains and that grains with finer fractions consist of sharp angular particles.

4.2 Sample preparation and description of the oedometric apparatus

The sand samples were poured into a thin-walled (1.3 mm) sample holder of 40 mm outer diameter (OD). The sand was meant to be placed in its loosest state and a target height of 12 mm, although a settling pressure of 0.2 MPa was applied before testing for the sake of sample homogenization. Even though a strict procedure of placement of the sand was followed, some scattering of the initial void ratio (from 0.72 to 0.85) was unavoidable. Nevertheless, as will be shown, this variation had little effect on the compressibility at high stresses (beyond the yield point). Fig. 3 illustrates the sample preparation.



Figure 3. Sample preparation of the one-dimensional compression tests.

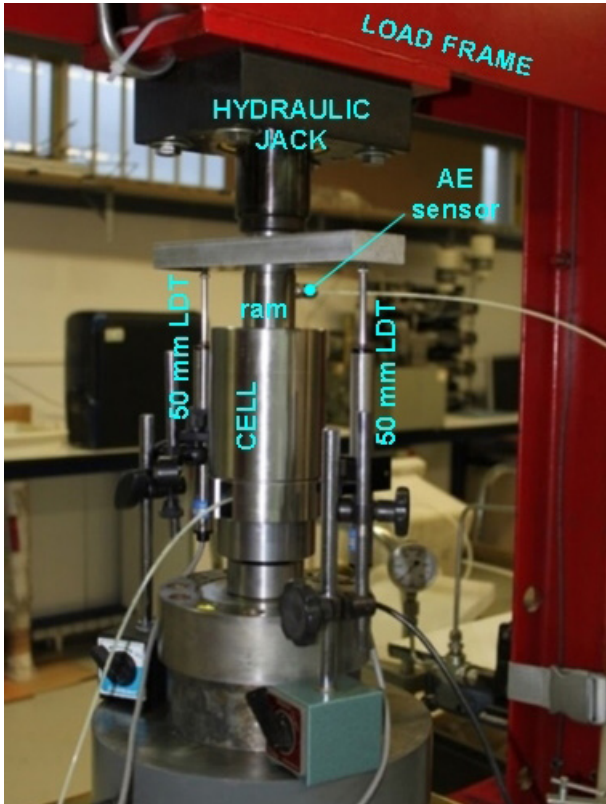


Figure 4. One-dimensional compression (oedometric) apparatus during testing.

The sample holder is fitted into an oedometric cell that consists of a stainless-steel cylinder with a 24.5-mm-thick wall. The oedometric cell is placed in a rigid load frame (Fig. 4). The axial load is applied by a servo-controlled hydraulic jack, acting at the selected loading rate. The axial displacement is measured by two external, averaged, LDT-type transducers, whereas the axial load is recorded by the built-in data-acquisition system of the hydraulic jack. Two band heaters are used to raise the temperature and keep it constant during the tests. They are connected to a PID temperature controller, and a PT100 sensor located in the middle of the inner cell wall was used. When necessary, thermal isolation blocks are placed around the cell (Fig. 5). A PAC-Micro200HF wideband acoustic emission sensor attached to the ram of the hydraulic jack records the acoustic events occurring within the sample (basically, crushing counts). The data are recorded with a Physical Acoustics Co. PCI-2 and the software AEwin for PCI r.2.1. As the sensor withstands just up to 177°C, acoustic emissions (AEs) data were recorded only for the tests at temperatures not exceeding 150°C.

4.3 Calibration for high temperatures and stresses

Several calibrations were carried out. An additional PT100 was required for the calibration of the tempera-

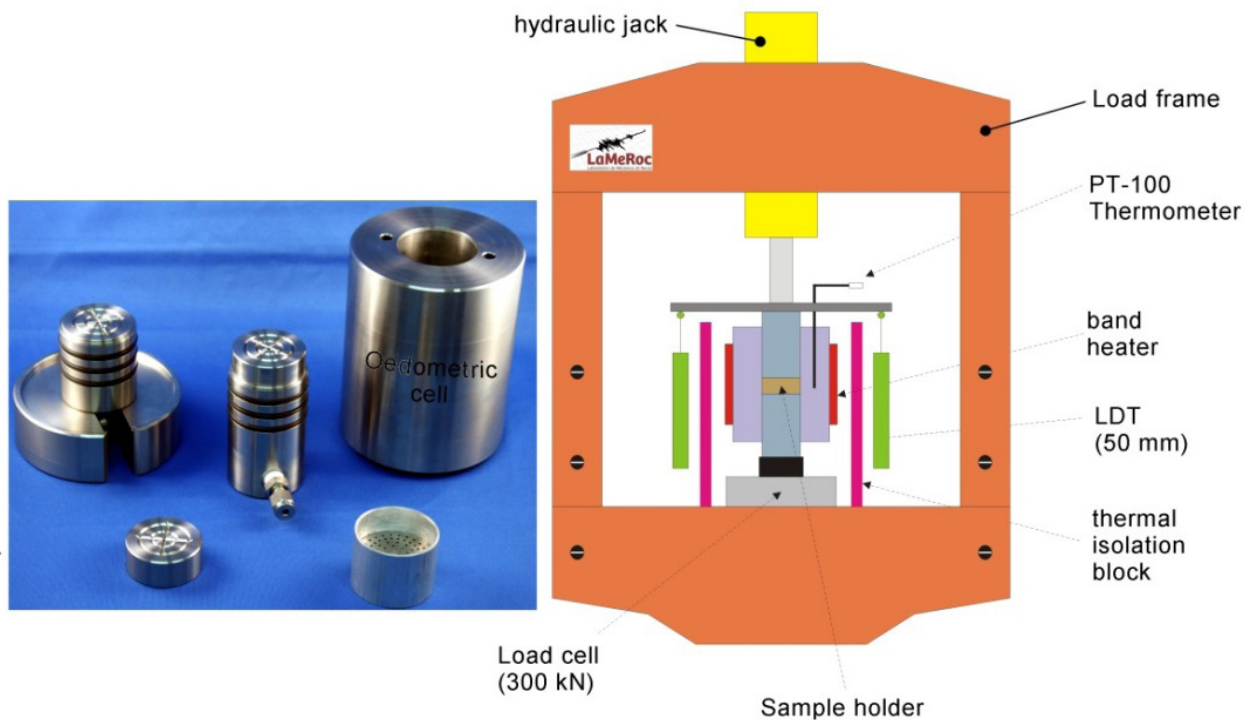


Figure 5. Layout of the oedometric apparatus.

ture. In the first stage of the temperature rise (from 25 to 109°C), an axial thermal expansion of 0.176 mm was recorded over the initial length (140.2 mm), while in a second stage (from 109 to 223°C), this expansion reached 0.284 mm.

Displacements were determined for the whole mechanical assembly (250 mm in height, including the load column) caused by the application of axial stress (from 0.1 to 50 MPa). A shortening of 0.613 mm was measured at 109°C, while a shortening of 0.534 was measured at 223°C. This difference in shortening (0.09 m) is attributed to the differential fitting of the O-rings into the oedometric cell. These calibration measurements yielded the linear thermal expansion coefficients, and the Young's moduli of the parts (perforated steel discs, positioning reference blocks, steel compression platens and refractory ceramic blocks to protect the load cell).

4.4 Stress paths of the oedometric tests

Prior to any loading, the sand samples were heated up to the target temperature. Once the samples reached it, the axial load was applied in three stages:

- a 10-step monotonic loading (0.2 / 1 / 2 / 3 / 4 / 6 / 10 / 15 / 20 / 25 / 30 MPa);
- a 4-step unloading/reloading loop (30 / 10 / 1 / 30 / 50 MPa);
- a 4-step monotonic unloading (50 / 30 / 15 / 5 / 1 MPa).

Each step of the loading increase or decrease was reached in seconds or a few minutes and maintained for 90 minutes. Hence, a whole oedometric test took approximately 28 h.

5 RESULTS

Fig. 6 shows 3 characteristic oedometric curves at different temperatures (25, 100 and 150°C) in which the AE data were recorded during the tests. Additionally, an oedometric curve at 250°C is included, even though the AE are not available due to the limitations of the sensor.

Compression curves show variations in the void ratio for the yield point followed by similar slopes, irrespective of the temperature of testing or the initial void ratio. Thus, Table 1 summarises the compression index (c_c) and the swelling index (c_s) obtained for all the oedometric tests carried out. The average compression index reached $c_c=0.294$ with a coefficient of variation as low as 0.1. These results compare reasonably well with those avail-

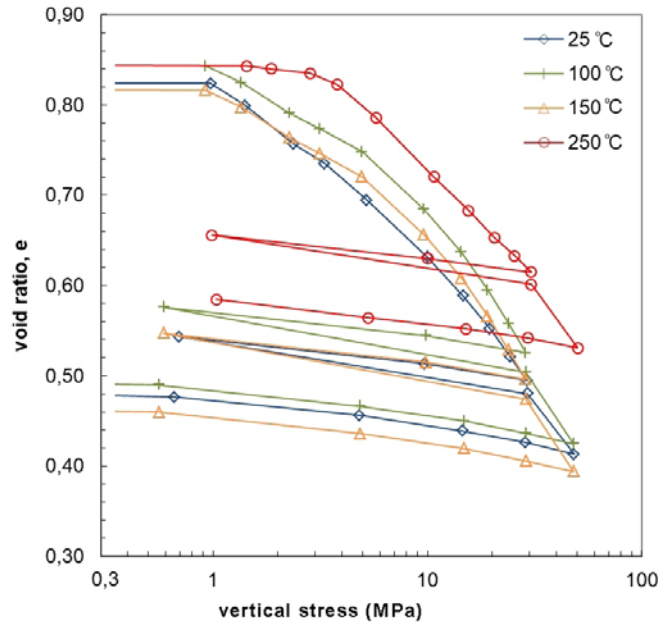


Figure 6. Representative oedometric curves for temperatures from 25 to 250°C.

Table 1. Compression indexes and swelling indexes for all the tests carried out.

	TEST	T (°C)	LOAD	UNLOAD	
			c_c	c_s	
LOW-MEDIUM TEMPERATURE	EDO-1	25	0.310	0.038	
	EDO-2		0.279	0.035	
	EDO-5		0.273	0.033	
	EDO-6		0.288	0.033	
	EDO-7		0.286	0.030	
	EDO-8		0.291	0.038	
	EDO-9		0.299	0.039	
	EDO-10		0.309	0.038	
	EDO-11		50	0.332	0.038
	EDO-12		60	0.257	0.030
	HIGH TEMPERATURE	EDO-13	100	0.306	0.032
		EDO-14		0.332	0.038
EDO-15		0.329		0.038	
EDO-16		0.332		0.038	
EDO-17		0.229	0.036		
EDO-18		150	0.287	0.037	
EDO-19			0.332	0.038	
EDO-20		200	0.276	0.037	
EDO-21			0.281	0.037	
EDO-22		250	0.249	0.032	

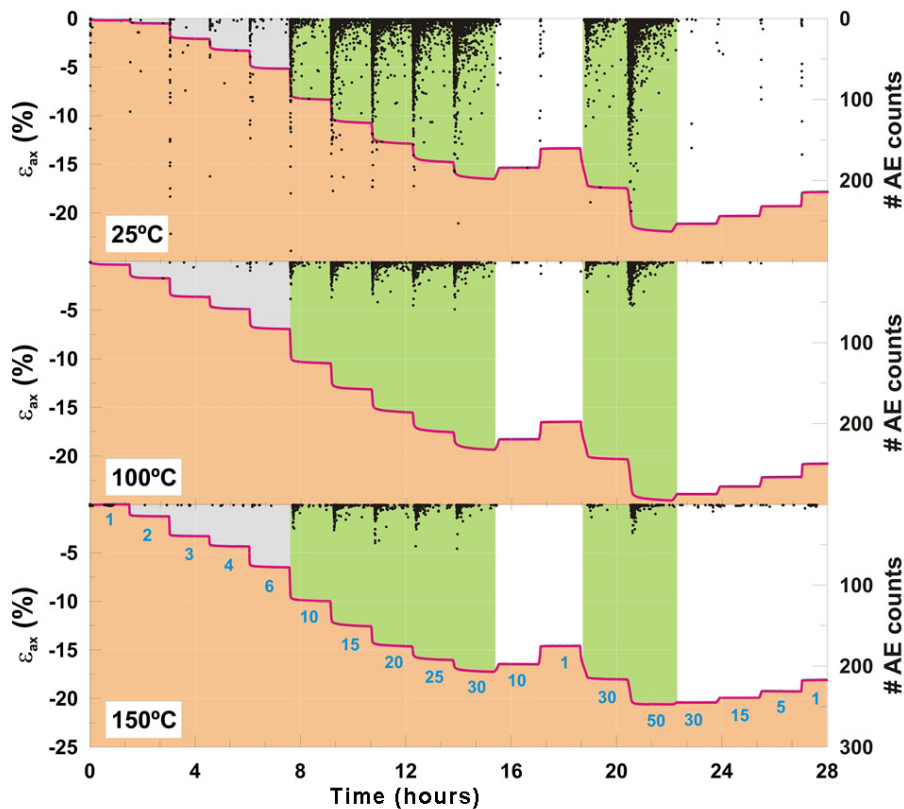


Figure 7. Acoustic emission data.

able in the literature [15, 27, 36 and 37]. In addition, the average swelling index $c_s=0.036$ is characteristic of the whole range of unloading to within 0.08.

Despite the similar results in the compaction and unloading results, the AE counts measured during the tests show a significant variation (Fig. 7). AEs at higher temperatures 1) are most frequent at the start of each loading ramp, 2) decay in frequency exponentially with time at each loading step, 3) are rare during unloading, and 4) exhibit lower counts at higher temperatures.

Such observations, together with the results of the grain size distributions before and after the tests (see Fig. 8), leave little doubt that the AEs correspond to the crushing events during the tests.

The tests carried out at room temperature underwent substantial grain failure: as shown in Fig. 8, the fines content increased from 18 even up to 55% and D_{50} (the grain size of the sand particles at 50% in the cumulative distribution) reduced in some cases by more than 50%. In contrast, the samples tested at higher temperatures revealed minor grain failure.

Finally, AEs prove to be useful for narrowing down the yield point. In this case, as the AE activity intensifies at

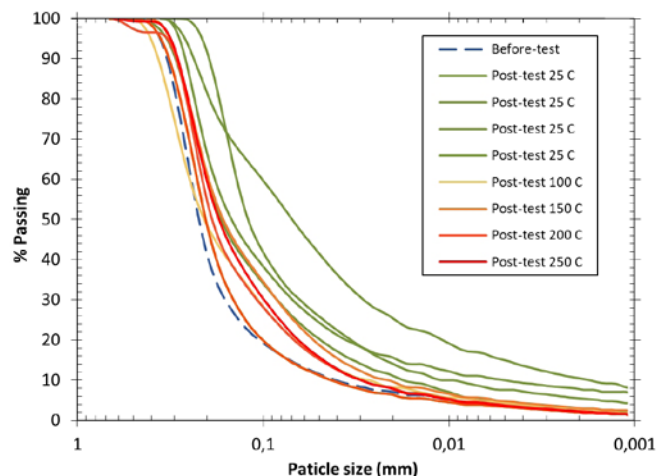


Figure 8. Grain size distribution curves before and after testing.

the range of 10 MPa, it appears reasonable to establish the yield point in that load step. Hence, according to Equation 7, a coordination number of 7.6 ± 0.5 at the yield point can be accepted. That range matches the expected value for dense sands $7.7 (C_n \approx 7.7$ for the maximum dry density considered $\approx 1700 \text{ kg/cm}^3$ and equivalent to a porosity $\approx 36\%$).

6 DISCUSSION

If the test temperature is raised, the macroscopic sand compressibility beyond the yield point remains unaffected, the AE activity decays, and changes in the particle size distribution are negligible. Therefore, it seems that phenomena other than grain-scale mechanical crushing alone must account for the compressibility at high temperatures.

On the one hand, with an increase of the temperature, the elastic parameters decrease [38] and so does the stress level at the tip of a crack or flaw (K_I). On the other hand, the fracture toughness, K_{IC} , increases [39 and 40]. Both circumstances make Equation 6 unlikely to hold and appears to be sufficient to explain the sharp decay of the AEs and the null change of the grain size distribution.

However, an SEM analysis (photomicrographs) of the sand grains, after being subjected to a stress of 14 MPa (according to the yield point) and at 150°C, proves the presence of incipient fractures, see Fig.9.

Furthermore, a detailed observation with an optical microscope reveals that the quartz grains contain fluid inclusions, not only in the syntaxial cement growth but in the detrital grains as well, Fig.10. These fluid inclusions are, in some cases, strongly aligned.

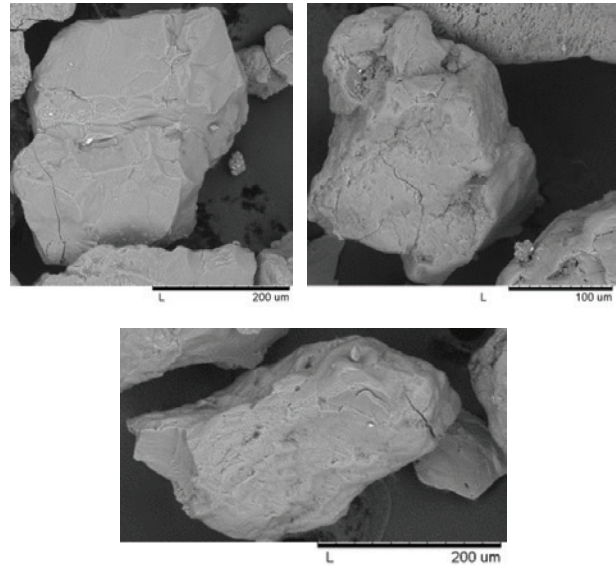


Figure 9. Incipient cracks on quartz grains tested at 150°C.

Thus, fluid inclusions, that are themselves flaws in the grain, seem to contribute to weakening its most overstressed region by the chemical rupture of the Si-O bonds. This process may counterbalance the decrease in the stress level due to the temperature rise in Equation 6. Such a phenomenon, known as stress-corrosion, is considered as the main mechanism of subcritical crack growth.

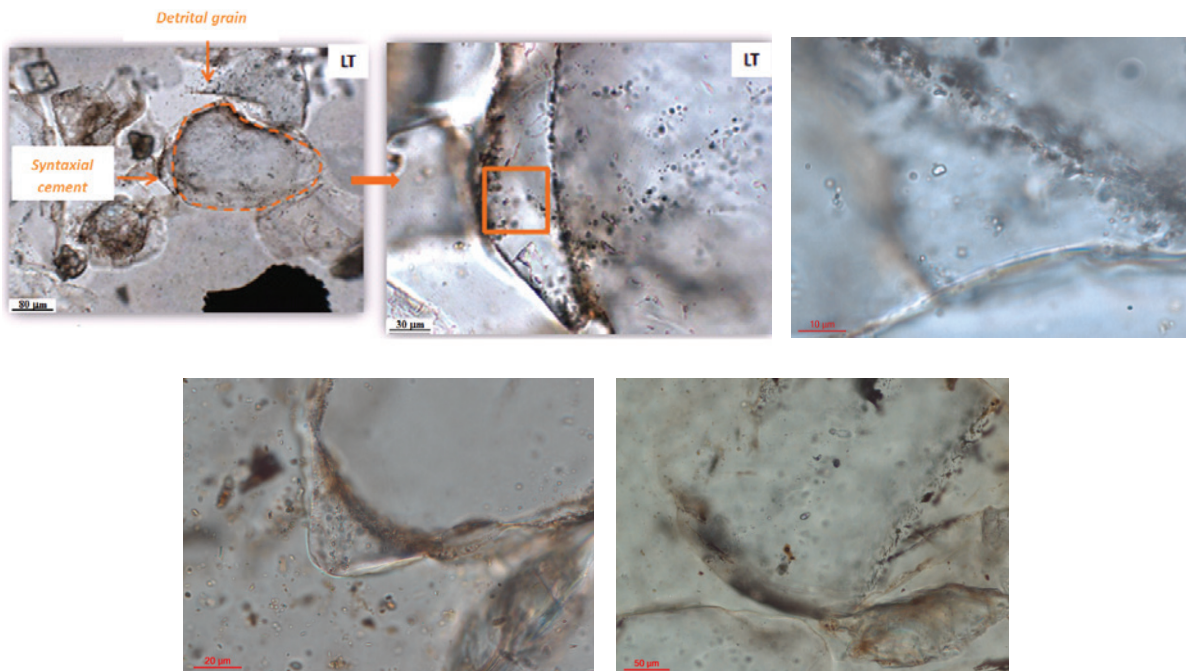


Figure 10. Fluid inclusions in quartz grains.

As a consequence, the subcritical crack growth rate, at high temperatures, does not release enough energy to generate sound waves (acoustic emissions), and some counts drop off as a result. Conversely, at room temperature, as the grain failure occurs once the effective critical stress for crushing is reached, the growth rate is faster, and the fast release of energy generates sound waves recorded as acoustic emissions.

7 CONCLUSIONS

Grain crushing is the fundamental source of the compressibility of sands subjected to high stresses at room temperature, although hardly any studies have been devoted to the effect of temperature. The presented oedometric tests revealed that the compressibility of quartz sand beyond the yield point is not affected either by the temperature or the initial void ratio; thus, all the oedometric curves follow a reasonably similar compression pattern ($c_c=0.294$ on average, with a coefficient of variation of 0.1).

Although the AE counts drop off and changes in the particle size distribution are negligible when the temperature is raised, the quartz grains subjected to high temperatures and stresses (150°C and 14 MPa) show incipient fractures.

A detailed study by optical microscope reveals fluid inclusions in the detrital grains, which suggests that subcritical crack growth may well be considered the cracking process of the grains at high temperature through stress-corrosion.

Finally, the fact that the compressibility remains unaffected by the temperature can be attributed to a change in the grain-scale mechanics: from critical rapid crack growth, at low temperatures, to fluid-sensitive subcritical cracking, at the higher temperatures, which is in good agreement with related works [41].

Acknowledgments

The authors would like to thank Repsol Technological Centre for granting permission to publish some of the results obtained in the tests shown in this paper.

REFERENCES

- [1] Lo, K.Y., Roy, M. 1973. Response of particulate materials at high pressures. *Soils and Foundations* 13(1), 61-76.

- [2] Vesic, A.S., Clough, G.W. 1968. Behaviour of Granular Materials under High Stresses. *Journal of Soil Mechanics and Foundations Division ASCE* 94(3), 661-688.
- [3] Lee, K.L., Farhoomand, I. 1967. Compressibility and crushing of granular soil in anisotropic triaxial compression. *Canadian Geotechnical Journal* 4(1), 68-86. doi:10.1139/t67-012
- [4] Bishop, A.W., Webb, D.L., Skinner, A.E. 1965. Triaxial test on soils at elevated cell pressure. In *Proceedings of the 6th International Conference on Soil Mechanics and Foundation Engineering*, Montreal, Canada, 1, pp 170-174.
- [5] Coop, M.R., Lee, I.K. 1993. The behaviour of granular soils at elevated stresses. In *Predictive Soil Mechanics. Proceedings of the Wroth Memorial Symposium*, Thomas Telford, London, UK, pp. 186-196.
- [6] Hardin, B.O. 1985. Crushing of soil particles. *Journal of Geotechnical Engineering* 11, 1177-1192.
- [7] Hagerty, M.M., Hite, D.R., Ullrich, C.R., Hagerty, D.J. 1993. One-dimensional high-pressure compression of granular media. *Journal of Geotechnical Engineering ASCE* 119(1), 1-18.
- [8] Yamamuro, J.A., Bopp, P.A., Lade, P.V. 1996. One-dimensional compression of sand at high pressures. *Journal of Geotechnical Engineering ASCE* 122(2), 147-154.
- [9] Lade, P.V., Yamamuro, J.A., Bopp, P.A. 1996. Significance of particle crushing in granular materials. *Journal of Geotechnical Engineering ASCE* 122(4), 309-316.
- [10] McDowell, G.R., Bolton, M.D. 1998. On the micro-mechanics of crushable aggregates. *Géotechnique* 48(5), 667-679. doi:10.1680/geot.1998.48.5.667
- [11] Nakata, Y., Hyodo, M., Hyde, A.F.L., Kato, Y., Murata, H. 2001b. Microscopic particle crushing of sand subjected to high pressure one-dimensional compression. *Soils and Foundations* 41(1), 69-82.
- [12] Borg, I., Friedman, M., Handin, J., Higgs, D.V. 1960. Experimental deformation of St. Peter Sand: a study of cataclastic flow. In *Rock Deformation* (D. Griggs, J. Handin Eds.), Geological Society of America Memoirs. 79, 133-192.
- [13] Zhang, J., Wong, T-F, Davis, D.M. 1990. Micro-mechanics of pressure-induced grain crushing in porous media. *Journal of Geophysical Research* 95(B1), 341-352.
- [14] Menendez, B., Zhu, W., Wong, T-F. 1996. Micro-mechanics of brittle faulting and cataclastic flow in Berea Sandstone. *Journal of Structural Geology* 18(1), 1-16.
- [15] Chuan, F.A., Kjeldstad, A., Bjarlykke, K., Hoeg, K.

2003. Experimental compression of loose sand: Relevance to porosity reduction during burial sedimentary basins. *Canadian Geotechnical Journal* 40(5), 995-1011. doi:10.1139/t03-050
- [16] Karner, S.L., Chester, F.M., Kronenberg, A.K., Chester, J.S. 2003. Subcritical compaction and yielding of granular sand. *Tectonophysics* 377(3-4), 357-381.
- [17] Karner, S.L., Chester, J.S., Chester, F.M., Kronenberg, A.K., Hajash, A. 2005. Laboratory deformation of granular quartz sand: Implications for the burial of clastic rocks. *American Association of Petroleum Geologists Bulletin* 89, 603-625.
- [18] Brzesowsky, R.H., Spiers, C.J., Peach, C.J., Hangx, S.J.T. 2014. Time-independent compaction behaviour of quartz sands. *Journal of Geophysical Research: Solid Earth* 119. doi:10.1002/2013JB010444.
- [19] Karner, S.L., Kronenberg, A.K., Chester, F.M., Chester, J.S., Hajash, A. 2008. Hydrothermal deformation of granular quartz sand. *Journal of Geophysical Research: Solid Earth* 113 (B05404). doi:10.1029/2006JB004710
- [20] Chester, J.S., Lenz, S.C., Chester, F.M., Lang, R.A. 2004. Mechanisms of compaction of quartz sand at diagenetic conditions. *Earth and Planetary Science Letters* 220, 435-451.
- [21] Chester, F.M., Chester, J.S., Kronenberg, A.K., Hajash, A. 2007. Subcritical creep compaction of quartz sand at diagenetic conditions: Effect of water and grain size. *Journal of Geophysical Research: Solid Earth* 112(B06203), 1-15. doi:10.1029/2006JB004317
- [22] Schutjens, P.M.T.M. 1991. Experimental compaction of quartz sand at low effective stress and temperature conditions. *Journal of the Geological Society* 148, 527-539. doi: 10.1144/gsjgs.148.3.0527
- [23] Wong, T-F. 1990. Mechanical compaction and the brittle-ductile transition in porous sandstones. *Geological Society Special Publication* 54, 111-122.
- [24] Wong, T-F., Baud, P. 1999. Mechanical compaction of porous sandstone. *Oil & Gas Science and Technology* 54(6), 715-727. doi:10.2516/ogst:1999061
- [25] Heard, J.C., Carter, N.L. 1968. Experimentally induced natural intergranular flow in quartz and quartzite. *American Journal of Science* 266, 1-42.
- [26] Golightly, C.G. 1990. Engineering properties of carbonate sands. PhD dissertation, Bradford University.
- [27] Nakata, Y., Kato, Y., Hyodo, M., Hyde, A.F.L., Murata, H. 2001a. One-dimensional compression behaviour of uniformly graded sand related to single particle crushing strength. *Soils and Foundations* 41(2), 39-51.
- [28] Leleu, S., Valdes, J.R. 2006. Crushing of sand mixtures. *Geomechanics and Geotechnics of Particulate Media*. Hyodo, Murata and Nakata (eds).
- [29] Drescher, A., De Josselin de Jong, G. 1972. Photoelastic verification for a model of the flow of granular material. *Journal of the Mechanics and Physics of Solids* 20, 337-351.
- [30] Gallagher, Jr. J.J. 1976. Fracturing of Quartz Sand Grains. *American Rock Mechanics Association, The 17th U.S. Symposium on Rock Mechanics (USRMS)*, 25-27.
- [31] Santamarina, J.C., Klein, K.A., Fam, M.A. 2001. *Soils and Waves: Particulate Materials Behavior, Characterization and Process Monitoring*. Wiley.
- [32] Mavko, G., Mukerji, T., Dvorkin, J. 2009. *The Rock Physics Handbook. Tools for Seismic Analysis of Porous Media*. Cambridge University Press, New York, United States of America.
- [33] Huber, M.T. 1904. Zur Theorie der Berührung fester elastischer Körper. *Annalen der Physik*. 319 (6), 153-163. <https://doi.org/10.1002/andp.19043190611>
- [34] Frank, F.C., Lawn, B.R. 1967. On the theory of Hertzian fracture. *Proceedings of the Royal Society of London. Series A, Mathematical and Physical Sciences*, 299(1458), pp. 291-306. doi: 10.1098/rspa.1967.0137
- [35] Field, W.G. 1963. Toward the statistical definition of a granular mass. In: *Proceeding of 4th Australia-New Zealand Conference on soil mechanics and foundation engineering*: 143-148.
- [36] McDowell, G.R., Humphreys, A. 2002. Yielding of granular materials. *Granular Matter*, 4(1), 1-8.
- [37] Mesri, G., Vardhanahuti, B. 2009. Compression granular materials. *Canadian Geotechnical Journal* 46(4), 369-392. doi:10.1139/T08-123
- [38] Pabst, W.E.G. 2013. Elastic properties of silica polymorphs-A review. *Ceramics-Silikáty* 57(3), 167-184.
- [39] Atkinson, B.K., Avdis, V. 1980. Technical Note. Fracture mechanics parameters of some rock-forming minerals determined using an indentation technique. *International Journal of Rock Mechanics and Mining Sciences & Geomechanics Abstracts* 17, 283-386.
- [40] Atkinson, B.K. 1984. Subcritical crack growth in geological materials. *Journal of Geophysical Research* 89(B6), 4077-4114.
- [41] Lenz, S.C. 2002. Acoustic emission and compaction creep of quartz sand at subcritical stress. MS Thesis. Texas A&M University (Unpublished).